Synthesis and characterization of Mn$_3$AC single crystals

A Dissertation for

PHY-651 Dissertation

Credits: 16

Submitted in partial fulfillment of Masters Degree

M.Sc in Physics in Solid State Physics

by

RUTUJA MANOJ JOSHI

22P0430033

305-227-430-565

20190206

Under the supervision of

DR. ELAINE T. DIAS

School of Physical and Applied Sciences

Physics Discipline

Goa University

May 2024

Examined by:

Seal of the School

DECLARATION BY STUDENT

I hereby declare that the data presented in this Dissertation report entitled, "Synthesis and characterisation of Mn_3AC single crystals is based on the results of investigations carried out by me in the Physics Discipline at the School of Physical and Applied Sciences, Goa University under the supervision of Dr. Elaine Dias and the same has not been submitted elsewhere for the award of a degree or diploma by me. Further, I understand that Goa University or its authorities will not be responsible for the correctness of observations / experimental or other findings given the dissertation.

I hereby authorize the University authorities to upload this dissertation on the dissertation repository or anywhere else as the UGC regulations demand and make it available to anyone as needed.

Name: Ms. Rutuja Manoj Joshi

Roll no: 22P0430033

Date: 08 May 2024

Place: Goa University

COMPLETION CERTIFICATE

This is to certify that the dissertation report "Synthesis and characterisation of Mn_3AC single crystals" is a bonafide work carried out by Ms Rutuja Manoj Joshi under my supervision in partial fulfilment of the requirements for the award of the degree of M.Sc in Physics at the School of Physical and Applied Sciences, Goa University.
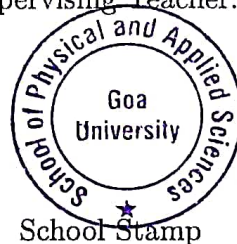
Name of the Supervising Teacher: Dr. Elaine T. Dias

Date: 08/05/2024

Signature:

School Stamp

Signature of Dean of the School:

Date: 8|5|24

Place: Goa University

<u>ACKNOWLEDGEMENT</u>

I would like to express my deepest gratitude to my supervisor, Dr. Elaine Dias, for her invaluable guidance, support, and encouragement throughout this dissertation. Her expertise, patience, and constructive feedback have been instrumental in shaping this dissertation. I would also like to thank Dr. Kaustubh Priolkar for his suggestions and Dr. Venkatesha Hathwar for doing the single crystal XRD experiment for me. I would also like to thank Elishka Vaz for giving me suggestions and helping me throughout the dissertation project. I would also like to thank all the PhD students for teaching me how to work in the lab and for their help during the project. Also, my heartfelt thanks to all the non-teaching staff for helping me whenever I needed their help.

Contents

List of Figures

List of Tables

<u>ABSTRACT</u>

Mn-based antiperovskites are interesting materials to study because they exhibit properties like giant-magnetoresistance, large magneto-caloric effect, giant negative thermal expansion, near-zero temperature coefficient of resistance, piezomagnetic effect etc. The polycrystalline and single compounds were studied to compare their characteristics. Studying single crystals of these compounds can provide more information about the compounds because they show unique properties because of their anisotropic nature due to the absence of defects. We could grow single crystals of Mn_3GaC and Mn_3SnC but their size was very small. The self-flux and slow cooling methods can be used to grow Mn-based antiperovskites.

Chapter 1

Introduction

1.1 Introduction

The solid state is divided into two categories amorphous solids and crystalline solids. Among these crystalline solids, there are two main subcategories polycrystals and single crystals. In the amorphous solids, the atoms are randomly arranged. Polycrystalline compounds are made up of many small crystals so they have grain boundaries, which is a defect, that might affect the properties of the compound. Single crystals are the purest form of the compounds which one can obtain because grain boundaries are absent and the lattice continuously repeats itself throughout the volume of the crystal. Single crystals show unique properties because of their anisotropic nature due to the absence of defects[1].
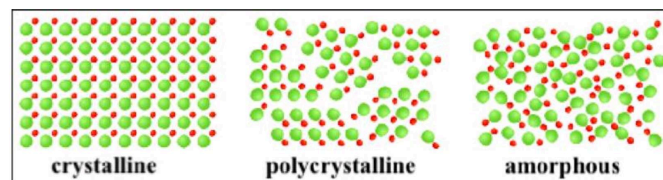
Figure 1.1: Single crystal, polycrystal and amorphous solids

1.2   Antiperovskites

Perovskites are a class of compounds with a general formula ABX_3 where A and B are cations and X is an anion. Antiperovskite compounds also have the same formula but cations replace anions and vice versa. A occurs at the corner of the cube, B occurs at the centre of the cube and X at the face-centred positions. They have a cubic structure with space group $Pm\bar{3}m$. The Mn-based antiperovskites are the most widely studied since they exhibit properties such as giant-magneto-resistance, large magneto-caloric effect, giant negative thermal expansion, near-zero temperature coefficient of resistance, piezomagnetic effect, etc [2]. Mn-based antiperovskites are more famous as they are comparatively easier to synthesise and show variations in the magnetic moment, magnetic structure and show magnetic transitions and also structural phase transitions.
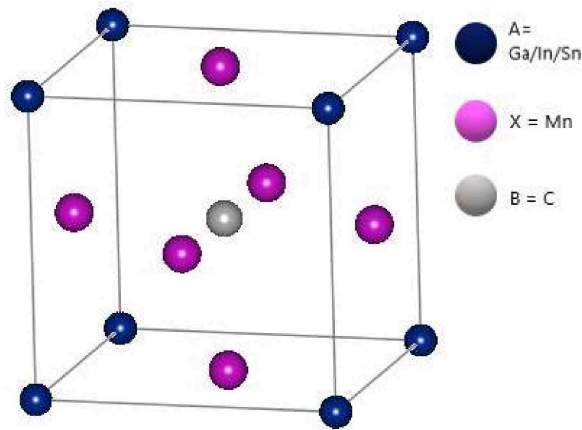
Figure 1.2: Antiperovskite structure

Mn_3GaC

Among these Mn-based antiperovskites, Mn_3GaC is the most widely studied compound where Ga sits at the A site, C at the B site and Mn at the X site. It is well known because it undergoes two magnetic transitions from paramagnetic to ferromagnetic via a second-order

transition at 243K and a first-order transition from ferromagnetic to antiferromagnetic at 163K. The temperature-dependent resistivity showed discontinuity at the transition temperatures. It has a cubic structure with space group $Pm\bar{3}m$ with lattice parameter a = 3.899 Å. The compound also shows the effect of field-induced transition when a magnetic field is applied. The lattice parameter varies with temperature, it continuously decreases with a decrease in temperature but it shows volume expansion at the first-order transition temperature. In addition, an inverse magneto-caloric effect is also seen at this temperature. The neutron diffraction data was recorded at 150K, at which the compound is in an antiferromagnetic state. Antiferromagnetic peaks appear in the neutron scattering experiment at this temperature. The magnetic structure gives propagation vector k = [1/2,1/2,1/2]. EXAFS measurements have shown distortion in Mn_6C octahedra that result in long and short Mn-Mn bond distances but the Mn-C bond shows very negligible variation across the magneto-structural transition.[2][3],[4]

Mn_3InC

Another compound studied in literature is Mn_3InC, which also forms a cubic structure with space group $Pm\bar{3}m$. Indium has the same electronic configuration as Gallium but it is bigger in size. The compound exhibits a broad magnetic transition from a paramagnetic to a ferromagnetic state at T_C 377 K. The variation of the lattice parameter with temperature showed a continuous decrease with a decrease in temperature and displayed no characteristic of first-order transition. It showed ferromagnetic behavior and no antiferromagnetic peaks were observed in the Neutron diffraction scattering experiment throughout the measured temperature range. Its magnetic structure diagram also confirms the AFM nature with a magnetic moment of 1.54 μ_B with k =[0,0,0].[5].

Mn$_3$SnC

Mn$_3$SnC is also an intermetallic compound and crystallises in cubic structure with space group Pm$\bar{3}$m. It has a transition temperature T$_C$ around 279 K, close to room temperature. Magnetisation measurements show a transition from a high-temperature paramagnetic state to a low-temperature magnetically ordered state with competing magnetic interactions. The resistivity shows metallic behavior with the change of slope near the transition temperature. It undergoes a cubic-to-cubic volume discontinuous transition at T$_C$. The magnetic structure diagram shows it has propagation vector k =[1/2,1/2,0]. XAFS measurements show that local structural disorder is present around the Mn atoms in the paramagnetic phase. This local strain may be due to the large size of the Sn atoms. This distortion leads to shorter and longer Mn-Mn bond distances that affect competition between nearest Mn-Mn antiferromagnetic interactions and next nearest Mn-Mn ferromagnetic interactions.[6],[7],[2].

Mn$_3$Ga$_{1-x}$Sn$_x$C

The size of the A-site atom plays an important role in the magnetostructural transition, this is observed in literature by study of doping Sn at A-site in Mn$_3$GaC, the Sn atom is bigger than the Ga atom and their electronic configuration is different. It was found that Sn atoms successfully replaced the Ga atoms. The study was done by doping Sn on Ga in the series $0 \leq x \leq 1$. It was observed that the doping does not alter the cubic structure and all the compounds formed with the space group Pm$\bar{3}$m. The compounds could be divided into three categories: Ga-rich, Intermediate and Sn-rich compounds. So, the Ga-rich compounds showed behaviour like that of Mn$_3$GaC, while the Sn-rich compounds showed behaviour like that of Mn$_3$SnC but, the intermediate compounds showed completely different behaviour. It was observed that the transition temperature increased across the series, and even the lattice parameter increased with an increase in doping concentration, with a suppressing antiferromagnetic ground state. The results obtained from XRD show the formation of a single phase at all concentrations. The compound with 50 % doping

showed fascinating behaviour, it showed the presence of both magnetic structures with k = [1/2,1/2,1/2] (Mn_3GaC) and k = [1/2,1/2,0] (Mn_3SnC) while it crystallised structurally in a single phase. The magnetisation measurements showed large splitting in ZFC and FC curves which is a characteristic of the magnetic glass state, this was confirmed by the AC susceptibility measurements, which indicated the formation of cluster glass. The AC susceptibility vs temperature plot showed a systematic shift towards higher temperature with increasing frequency, a decrease in amplitude with increasing frequency is a characteristic of a magnetic glassy state. So, magnetically it showed the formation of clusters, either rich in Ga or rich in Sn but structurally it showed a single phase. [8][9][10]

$Mn_3Sn_{1-x}In_xC$

Another series studied by doping at A site is doping of Indium on Mn_3SnC, here Sn and In are of the same size but their electronic configuration is not the same. This series also showed Sn-rich compounds, which showed behaviour like Mn_3SnC, and In-rich compounds, which showed behaviour like that of Mn_3InC and intermediate compounds exhibited different behaviour. The lattice parameters were almost constant across the series. Among the intermediate compounds, compound with 50% doping showed the presence of magnetic structures with k = [1/2,1/2,0] (Mn_3SnC) and k = [0,0,0] (Mn_3InC), while structurally it showed a single phase. [2]

The objectives of this project are to synthesis and characterisation of polycrystalline compounds Mn_3GaC, Mn_3InC, $Mn_3Ga_3In_3C$ and single crystals Mn_3GaC, Mn_3InC, Mn_3SnC and $Mn_3Ga_3In_3C$. Chapter 2 contains the sample preparation method and the details of various techniques used to characterise the samples. Chapter 3 presents the results and discussion.

Chapter 2

Methods

The compounds prepared are antiperovskite compounds with formula ABX_3 (for polycrystalline samples), elements taken in molar ratio 1:1:3 and A_2BX_4 (for single crystal samples), elements taken in molar ratio 2:1:4. All the prepared compounds have C (carbon) at the B site, Mn (Manganese) at the X site, and Ga/In/Sn at the A site.

It is difficult to grow metallic single crystals compared to organic single crystals. The single crystal compounds are prepared using the self-flux method where Mn and A site atom were used as a flux, the molecular formula used was A_2BX_4 as reported in the literature[11] but followed by a slow cooling process, the compounds were cooled at the rate of 1°C per hour. 20% excess carbon was taken to avoid carbon deficiency in the compounds. Flux or high-temperature solution growth involves the growth of the single crystals from molten salt solvent. The flux is a molten salt solvent at high temperature with the solute being dissolved. The flux helps the crystal grow below the solute's melting point. Because of slow cooling the crystals get considerable time to grow in a particular direction unless altered by any other nucleation center. This ensures the production of large crystals.

2.1 Calculations

The samples prepared are: Mn_4In_2C, Mn_4Sn_2C, Mn_4Ga_2C, Mn_4GaInC, $Mn_3Ga_{0.5}In_{0.5}C$, Mn_3InC, Mn_3GaC. Calculations for samples prepared:

Sample 1	Mn_4In_2C	Mn_4In_2C	461.403
	Calculation for 1g	Calculation for 2g	Actual weights taken for 2g
Mn	0.4763	0.9525	0.9525
In	0.4977	0.9954	0.9955
C	0.0260	0.0521	
20 % excess C	0.0312	0.0625	0.0625

Table 2.1: Calculations for Mn_4In_2C

Sample 2	Mn_4Sn_2C	Mn_4Sn_2C	469.143
	Calculation for 1g	Calculation for 2g	Actual weights taken for 2g
Mn	0.4684	0.9368	0.9367
Sn	0.5060	1.0119	1.0119
C	0.0256	0.0512	
20 % excess C	0.0307	0.0614	0.0614

Table 2.2: Calculations for Mn_4Sn_2C

Sample 3	Mn_4Ga_2C	Mn_4Ga_2C	371.203
	Calculation for 1g	Calculation for 2g	Actual weights taken for 2g
Mn	0.5920	1.1840	1.1840
Ga	0.3756	0.7513	0.7515
C	0.0324	0.0647	
20 % excess C	0.0388	0.0777	0.0777

Table 2.3: Calculations for Mn_4Ga_2C

Sample 4	Mn_4GaInC	Mn_4GaInC	371.203
	Calculation for 1g	Calculation for 2g	Actual weights taken for 2g
Mn	0.5278	1.0557	1.0557
Ga	0.1675	0.3349	0.3350
In	0.2758	0.5516	0.5516
C	0.0288	0.0577	
20 % excess C	0.0346	0.0692	0.0693

Table 2.4: Calculations for Mn_4GaInC

Sample 5	$Mn_3Ga_{0.5}In_{0.5}C$	$Mn_3Ga_{0.5}In_{0.5}C$	371.203
	Calculation for 1g	Calculation for 2g	Actual weights taken for 2g
Mn	0.6125	1.2250	1.2251
Ga	0.1295	0.2591	0.2592
In	0.2133	0.4267	0.4267
C	0.0446	0.0893	
20 % excess C	0.0536	0.1071	0.1071

Table 2.5: Calculations for $Mn_3Ga_{0.5}In_{0.5}C$

Sample 1	Mn_3InC	Mn_3InC	291.645
	Calculation for 1g	Calculation for 2g	Actual weights taken for 2g
Mn	0.5651	1.1302	1.1303
In	0.3937	0.7874	0.7874
C	0.0494	0.0988	
20 % excess C	0.0494	0.0988	0.0989

Table 2.6: Calculations for Mn_4In_2C

Sample 3	Mn_3GaC	371.203
	Calculation for 1g	Actual weights taken for 1g
Mn	0.6685	0.6686
Ga	0.2828	**0.7515**
C	0.0487	
20 % excess C	0.0585	0.0586

Table 2.7: Calculations for Mn_3GaC

2.2 Sample preparation

Cleaning of Mn: The purity of Mn used was 99.9% (metal basis). The metal cleaner was taken in a beaker until the Mn pieces were completely submerged. Next, the beaker is kept in the ultrasonicator for 15 minutes to vibrate the pieces and remove the rust. Next, these pieces were wiped and put in the isopropyl alcohol. The same procedure was repeated until the pieces of Mn were completely shining. Once the Mn pieces became completely shiny, they were ground into fine powder.

Indium: The purity of Indium used is 99.99%. Indium was available in small cube-like forms cut into fine pieces using a blade. Gallium: The purity of Gallium used was 99.99%(metal basis). Gallium has a melting point of 29.7°C so it should be stored at lower

Figure 2.1: Steps involved in sample preparation

temperatures. Gallium was melted small beads were made and then weights were measured. Tin: The purity of Tin used was 99.99% (metal basis). Tin metal was in the form of tin shots, these shots were pounded into thin sheets and then cut into fine pieces. Carbon (graphite): Graphite is available in powder form. The purity of graphite is 99.9995% (metal basis).

All these elements were weighed according to the calculated weights as mentioned above. Mn powder and graphite were first ground until a homogeneous mixture was formed in a mortar and pestle. Next, the A-site elements(Ga, In, Sn) were mixed with this powder mixture.

Once properly mixed, this mixture was poured into the quartz tube. All the compounds were in powder form, except Mn_3InC single crystal and Mn_3SnC single crystal which were pressed into pellets using the KBr pellet press and the pelletiser. The quart tube is then sealed, vacuum evacuated, and kept for sintering in the furnace. Heat bricks are used in the furnace to ensure the heat supply is equal on all sides of the compound.

2.3 Heat Treatment

The heating program for polycrystalline and single-crystal samples was as follows: All the compounds were ramped from room temperature to 800 °C at the rate of 1°per minute and were dwelled for 2 days, then they were ramped to 877 °C from 800 °C at the rate of 1.5°C per minute and then dwelled for 5 days. The polycrystalline compounds were furnace cooled whereas the single crystals were cooled at the rate of 1°C per hour, using the slow cooling technique to grow single crystals. The procedure we followed is modified, in literature [11] had prepared compound Mn_4Ga_2C by using solid-state reaction method in powder form, it was sintered at 800°C then ground pressed into a pellet and reintroduced in the furnace, this procedure was repeated three times.

2.4 X-ray diffraction

X-ray diffraction or XRD is a non-destructive analytical technique used to analyse physical properties such as phase composition, crystal structure, and orientation of powder, solid, and liquid samples[12],[13]. It follows Bragg's law:
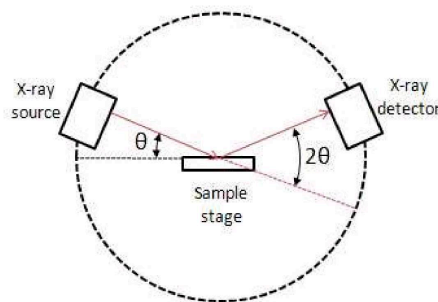
$$2dsin\theta = n\lambda \qquad (2.1)$$

Figure 2.2: Schemetic diagram of XRD

A beam of electrons is made incident on the sample where the electron beam knocks off

an electron from the k-shell of the atom, the k-shell vacancy is filled by an electron from the l shell which results in K_α radiation. When X-rays encounter any form of matter, they are partly reflected and partly absorbed. When the reflected X-rays satisfy Bragg's law, they produce constructive interference.

2.4.1 Powder XRD

The instrument geometry of the diffractometer used for powder XRD measurements had the sample at a fixed position and both x-ray beam and detector move which is called as $\theta - \theta$ arrangement. A Rigaku X-ray diffractometer was used to perform the XRD measurements. The radiation used is Cu-K_α radiation,wavelength $\lambda = 1.540560\text{Å}$.
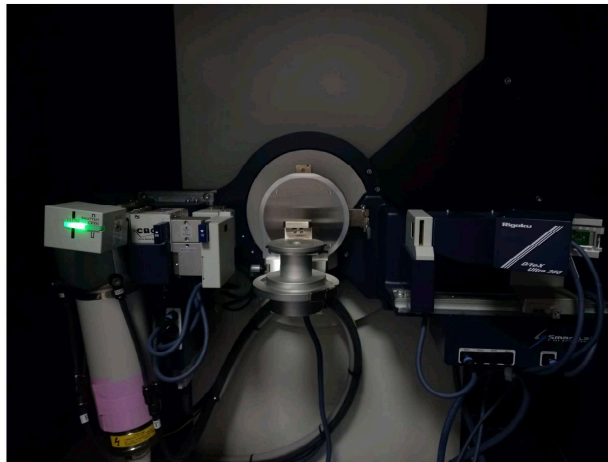

Figure 2.3: Rigaku diffractometer used for powder XRD measurements

The samples used for the X-ray diffraction experiment were first cooled to room temperature and then ground into fine powder for the measurement. To verify the formation of phases and purity of the samples formed, the data is refined by two methods Le Bail refinement and Rietveld refinement using the FULLPROF suite refinement program[14]. To calculate the intensities of the peaks a file was generated by using space group Pm$\bar{3}$m, site occupancies and approximate value of the lattice parameter. The integrated area of the peak

is proportional to the Bragg Intensity I_{hkl}.

$$I_{hkl} = |F_k|^2$$

Calculated intensity depends on $|F_k|^2$, along with contribution from neighbouring Bragg reflection and background profile.

$$F_{hkl} = \sum_i N_i f_j exp[2\pi i(hx_j + ky_j + lz_j] \times exp[-8\pi^2 U^2 sin^2\theta/\lambda^2]$$

Where f is atomic scattering factor, N is site occupancy. Least square refinement: where the entire powder diffraction pattern taken is taken as a whole a best fit of this with the entire calculated pattern is carried out.

$$S_y = \sum_i w_i(y_i - y_{ci})^2$$

where $w_i = 1/y_i$, y_i= observed intensity, y_{ci}= calculated intensity

$$Y_{ci} = s \sum_k L_k |F_k|^2 \phi(2\theta_i - 2\theta_k) P_k A + y_{bi}$$

where s = scale factor, k = Miller indices(hkl), ϕ=reflection profile function, A = absorption factor, L_k=Lorentz, polarization and multiplicity factor, P_k=Preferred orientation function, F_k=Structure factor for the Kth Bragg reflection, Y_{bi}=Background intensity at the ith step. Criteria for fit are as follows:

$$R_F = \sum |(I_{k(obs)})^{1/2} - (I_{k(calc)})^{1/2}|/ \sum (I_{k(obs)})^{1/2}$$

$$R_B = \sum |(I_{k(obs)}) - (I_{k(calc)})|/ \sum (I_{k(obs)})$$

$$R_p = \sum |(Y_{i(obs)}) - (Y_{i(calc)})|/ \sum (Y_{i(obs)})$$

$$R_{\mathrm{wp}} = \left[\sum w_{\mathrm{i}}((Y_{\mathrm{i(obs)}}) - (Y_{\mathrm{i(calc)}}))^2 / \sum w_{\mathrm{i}}(Y_{\mathrm{i(obs)}})^2\right]^{1/2}$$

$$R_{\mathrm{e}} = \left[N - P / \sum w_{\mathrm{i}}(Y_{\mathrm{i(obs)}})^2\right]^{1/2}$$

$$S = R_{\mathrm{wp}}/R_{\mathrm{e}} = \chi$$

where R_F= Residual structure factor, R_B = Residual Bragg, R_p = Residual pattern, R_{wp}= Residual weighted pattern, R_e= Residual expected, S = Goodness of fit[15].

2.4.2 Single crystal XRD

Bragg's equation that specifies if a crystal is rotated within a monochromatic x-ray beam, such that every conceivable orientation of the crystal relative to the beam is achieved, each set of planes will have the opportunity to satisfy the Bragg equation and to give rise to reflection. To solve a crystal structure it is necessary to record a large number of reflections. The crystals were separated using an optical microscope and selected for the single crystal XRD refinement. One among these was mounted on the loop and placed on the goniometer head. The crystal was adjusted properly using the video camera. Mo K_α radiations were used, wavelength $\lambda = 0.71073$Å. From the markers on the screen and rotating the crystal, with the help of a video camera, it can be said that the size of the crystal is about 50 microns. Steps involved in the single crystal determination are:

1. Select a suitable crystal

2. Crystal system and unit cell determination

3. Full data set collection

4. Bravais lattice

5. Space group

6. Construct an electron density map

7. Locate atom positions

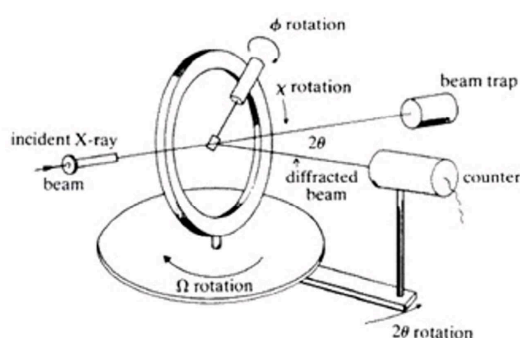8. Structure refinement

Single crystal XRD setup:

Figure 2.4: Single crystal XRD setup

Bruker diffractometer is used for the experiment. It has 4 circle geometry, full 360°rotations about ω and ϕ axes. Rotation about κ axis reproduces a quarter circle about χ axis. The other two angles are 2θ and Ω. One single piece of a single crystal of size between 10 microns to 300 microns is enough to obtain reflections. The sample is mounted on a thin loop and is placed on the goniometer head. The crystal is then adjusted to the centre with the help of a video camera connected to the screen. We get the hkl reflections from the planes of the single crystal and data is recorded. We can get lattice parameters and Bravias lattice, we can choose the space group and data reduction can be done using the APEX software by Bruker. We get the stricture solution from ShelXL software. Final refinement is done using Olex2.0 software.

2.5 Four Probe Resistivity

Four-probe resistivity measurement is a technique used to measure resistivity of the samples that have low resistance values. The resistivity is calculated using the formula:

$$\rho = R\frac{A}{l}$$

The setup consists of four equally spaced probes of copper. The voltmeter is attached to the two middle probes and the ammeter is attached to the outer two probes. First pellets of samples are prepared and then cut into rectangular bars to use for the resistivity measurements. These rectangular bars are then mounted on the four probes using G-varnish.

Figure 2.5: Sample stuck on four probes set up

Electrical contacts between the sample and the four probes are made using silver paint. The measurements are done in the temperature range 50 K to 450K and resistance was measured for warming and cooling cycles. The measurements were done using a conventional DC four-probe setup and a close-cycle refrigerator. Also, the LakeShore 325 temperature controller, Keithley 6221 DC and AC current source were used to pass 10 mA current, and Keithley voltmeter 2182A nanovoltmeter was used.

Figure 2.6: Instrument used for SEM measurements

2.6 SEM

Scanning Electron Microscopy (SEM) is a technique used to enlarge small features of compounds that cannot be seen with the naked eye. It works like a normal microscope but uses a high-energy electron beam to image the sample. Since the X-rays have a small wavelength it becomes advantageous to resolve the fine features of the compounds, closely spaced specimens can be magnified. It is a tool that provides information about the surface or near-surface structure, composition, and defects in bulk materials. The SEM instrument consists of an electron column, and specimen chamber, which are kept under vacuum, and computer controls. The electron column consists of an electron gun which generates the electron beam[16],[17]. The instrument used for SEM measurements is Carl-Zeiss EVO 18 Special Edition.

2.7 DSC

Differential Scanning Calorimetry or DSC is a technique where the calorimeter can measure the amount of heat absorbed or released when the sample undergoes a transition, it measures the amount of heat required to maintain both at the same temperature. In this
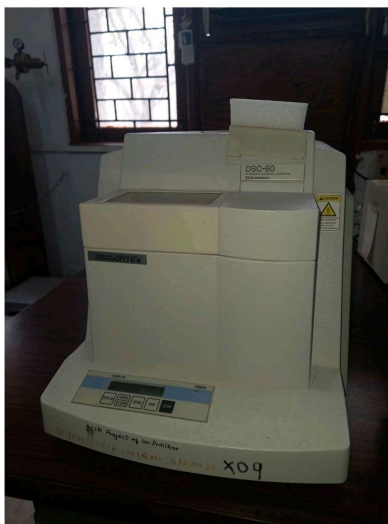
Figure 2.7: Instrument used for DSC measurements

technique, a reference aluminum pan and a pan crimped with the sample are maintained at the same temperature. The difference in the amount of heat required to increase or decrease the temperature as a function of temperature is measured. The exothermic reactions are observed as peaks and the endothermic reactions are observed as dips. The instrument used is the Shimadzu DSC-60. Approximately 9-10mg pieces of the pellet were used in the experiment.[18]

Chapter 3

Results

The polycrystalline compounds studied are Mn_3GaC, Mn_3InC, and the intermediate compound $Mn_3Ga_{0.5}In_{0.5}C$ and the Single crystal compounds studied are Mn_3GaC, Mn_3InC, the intermediate compound $Mn_3Ga_{0.5}In_{0.5}C$ and, Mn_3SnC.
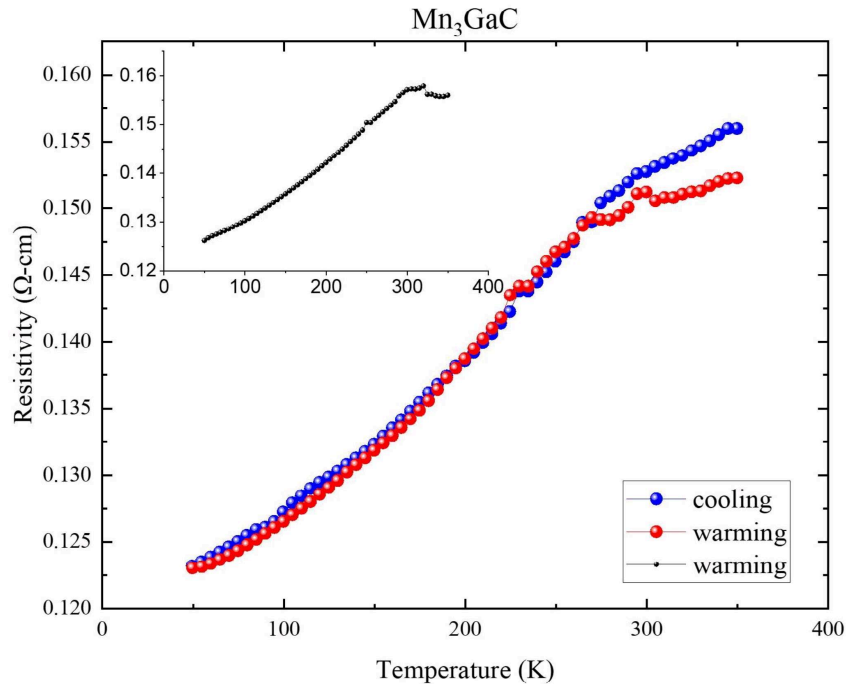
3.1 Mn_3GaC

3.1.1 Le Bail and Rietveld refinement

The Le Bail and Rietveld refinement of room temperature XRD patterns of Mn_3GaC are shown in figures 3.1 and 3.2. The data was recorded from $2\theta = 20$ °to 80 °in steps of 0.02°using Cu K_α radiation, wavelength $\lambda = 1.540560$Å.

Le Bail refinement shows that the sample crystallizes in the simple cubic phase as reported with space group $Pm\bar{3}m$ and the lattice constant is a $= 3.89447(3)$Åalong with impurity of graphite. Also, from the Rietveld refinement lattice constant of Mn_3GaC (90.32%) was found to be a $= 3.895451(3)$Åwith impurity of C(9.68%) (graphite). The lattice constant is less than that reported in the literature for the stoichiometric compound, it is closer to the carbon deficient. compound[3].
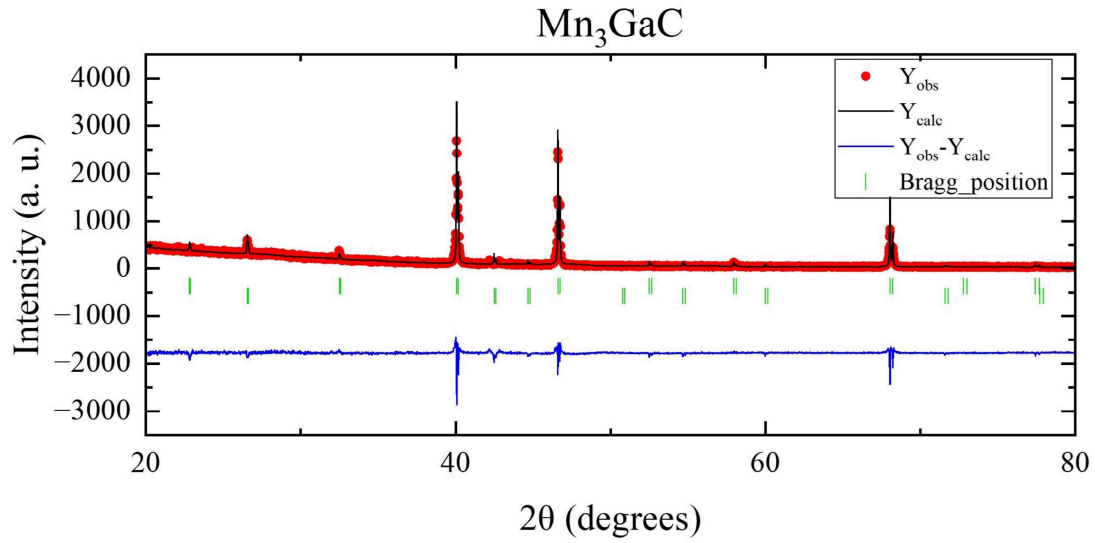
Figure 3.1: Le Bail refinement for Mn$_3$GaC
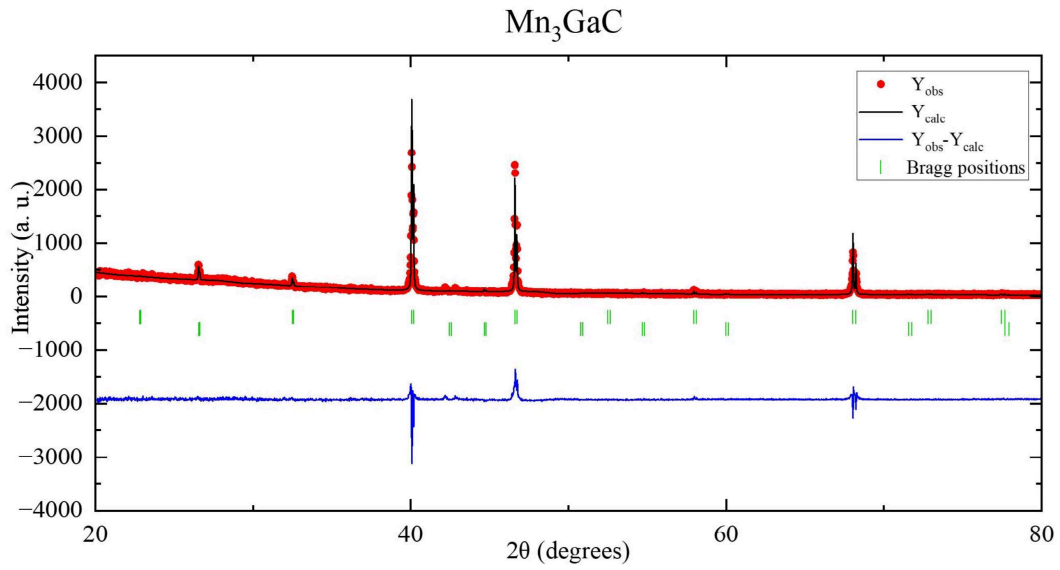
Figure 3.2: Rietveld refinement for Mn$_3$GaC

3.1.2   Resistivity

In order to understand transport properties resistivity measurements were done in the temperature range 50K to 350K shown in the figure 3.3. The compound overall showed a metallic behaviour with a sharp decrease in resistivity. This behaviour of resistivity is exactly similar

19

Figure 3.3: Resistivity vs Temperature plot for Mn_3GaC

to that reported earlier for $Mn_3GaC_{0.8}$ polycrystalline sample[3].

3.2 Mn_3InC

3.2.1 Le Bail and Rietveld refinement

The XRD patterns of the sample were recorded at room temperature using Cu K_α radiation, wavelength $\lambda = 1.540560$Åare shown in the figures below 3.4 and 3.5. The data was recorded from $2\theta =20°$to 80°in steps of 0.02°.

From the Le Bail and Rietveld refinement, figures 3.4 and 3.5 respectively, it was confirmed that Mn_3InC (22.35%) crystallizes in a cubic structure as reported in the literature, with space group Pm$\bar{3}$m and lattice parameter a = 3.99441(3)Å(Le Bail refinement) and a = 3.99554(5)Å(Rietveld refinement). The expected outcome was the compound would form a single phase but, impurities of C(70.3%), In(4.28%), and MnO(3.10%) were formed. The intensity of the carbon peak found is quite high.
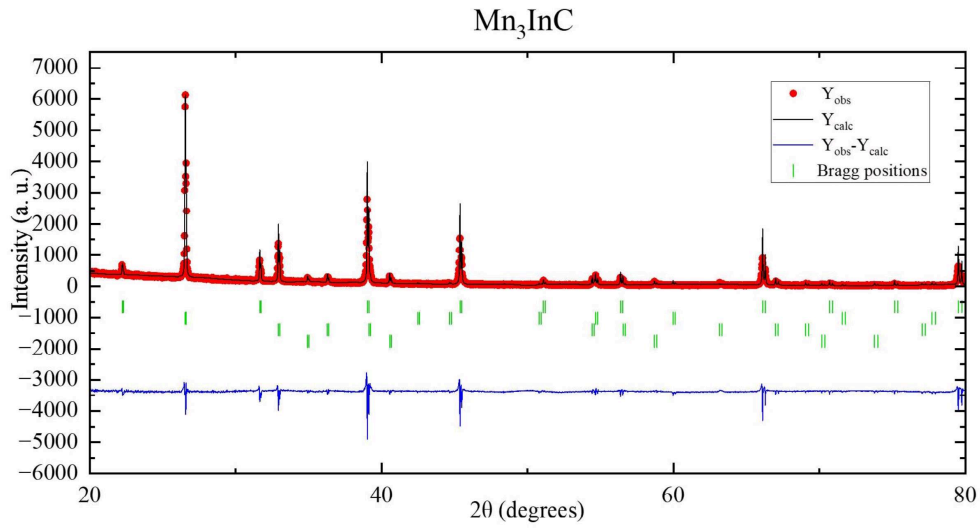
Figure 3.4: Mn₃InC Le Bail refinement
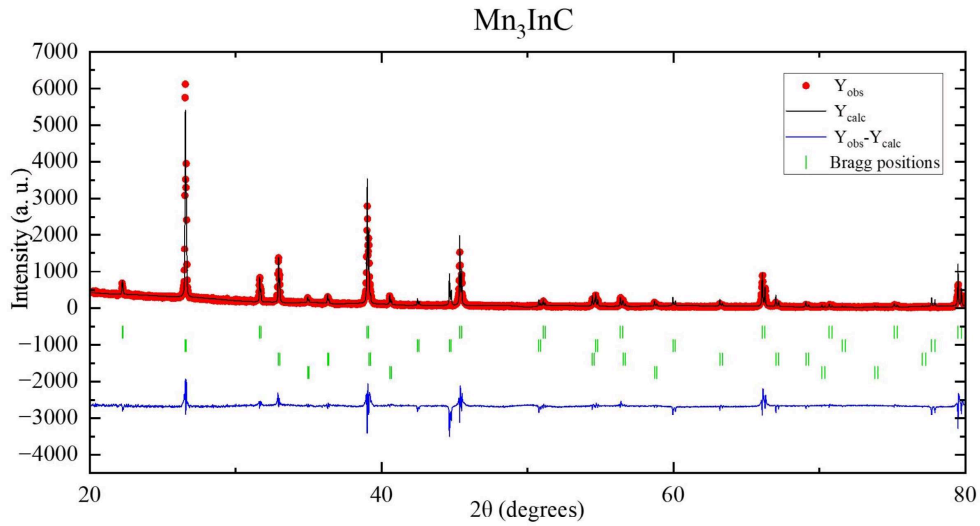
Figure 3.5: Mn₃InC Rietveld refinement

3.2.2 Resistivity

To study the transport properties temperature dependent resistivity measurements were done in the temperature range 50K to 450K3.6. The resistivity vs temperature plot shows a
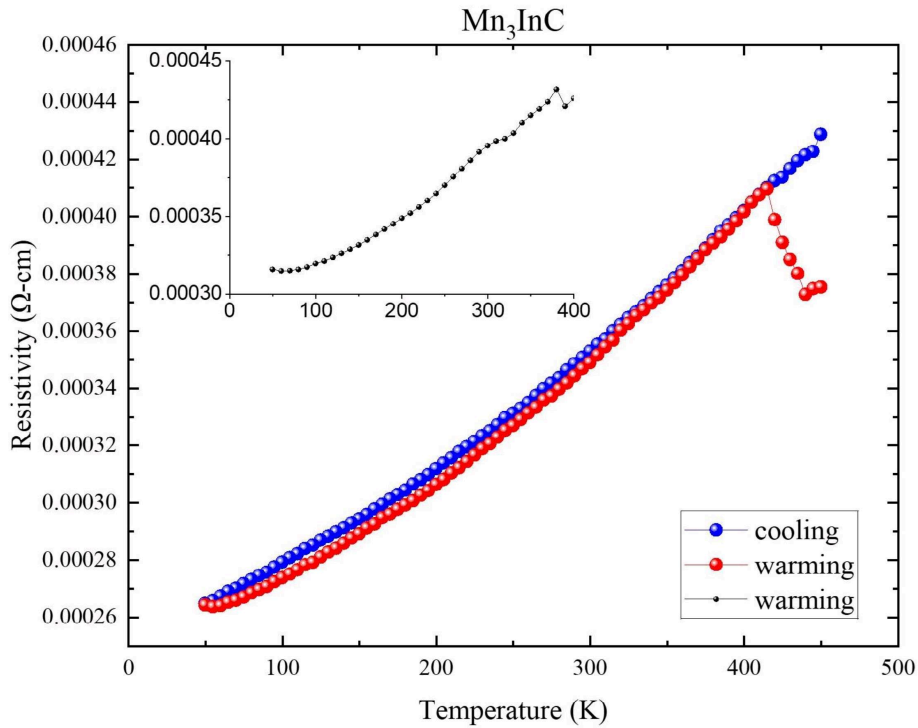
Figure 3.6: Resistivity vs Temperature plot for Mn$_3$InC

transition around 370K in the first warming cycle which is not seen in the other two cycles. Also in the second warming cycle resistivity suddenly drops approximately at 400K. Overall it shows a metallic behaviour.

3.3 Mn$_3$Ga$_{0.5}$In$_{0.5}$C

3.3.1 Le Bail and Rietveld refinement

This is the intermediate compound, the XRD patterns were recorded at room temperature, from 2θ =20°to 80°in steps of 0.02°using Cu K_α radiation, wavelength $\lambda = 1.540560$Å.

From both Le Bail 3.7 and Rietveld refinements 3.8, it was confirmed that the compound crystallizes in cubic phase as reported in the literature with space group Pm$\bar{3}$m along with impurities of C(1.82%) and Indium(1.60%). The lattice parameter from Le Bail refinement is a = 3.94741(5)Åand that obtained from Rietveld is a = 3.94687(5) Å. From Rietveld analysis,
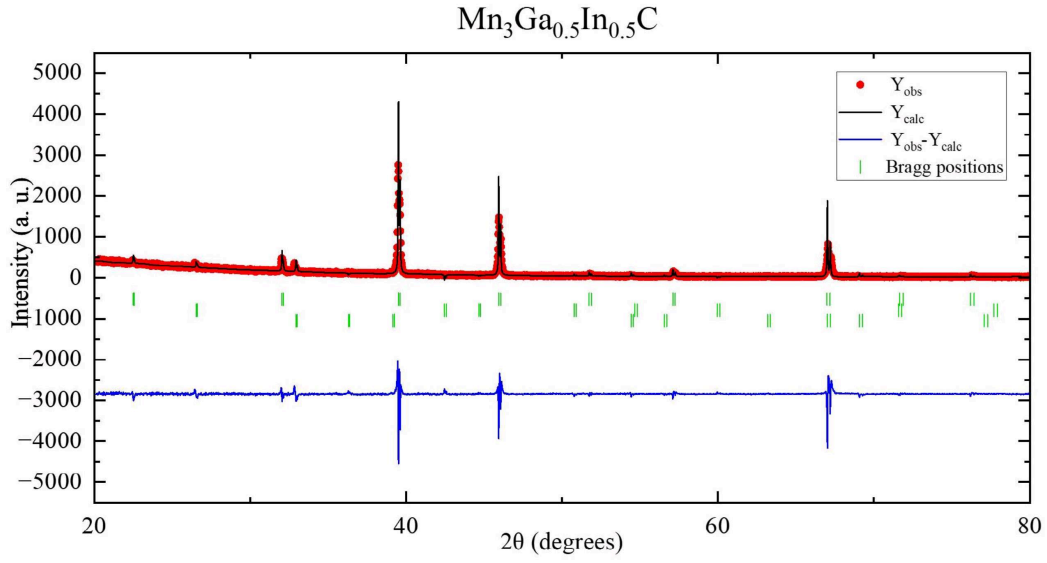
Figure 3.7: Le Bail refinement for Mn$_3$Ga$_{0.5}$In$_{0.5}$C
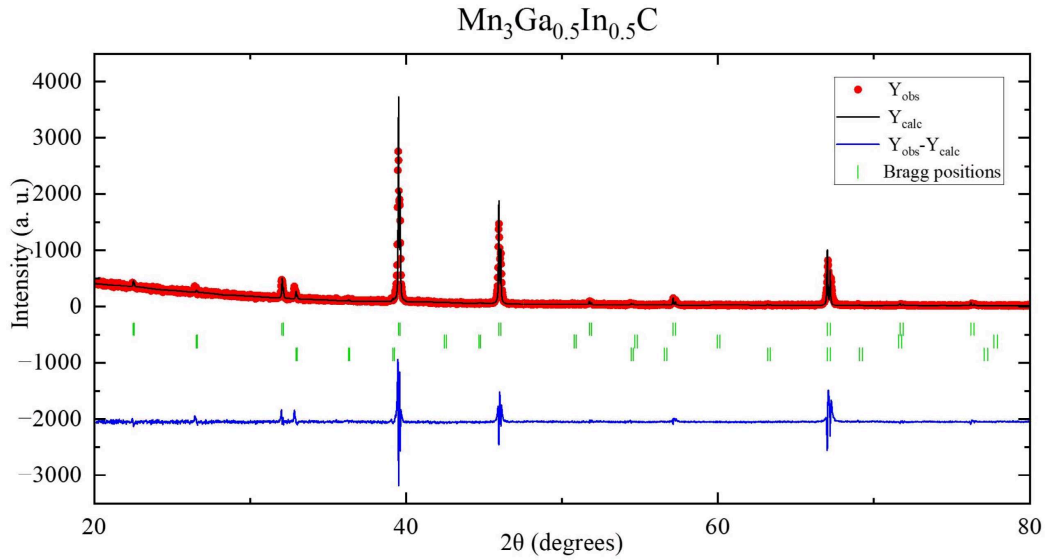
Figure 3.8: Rietveld refinement for Mn$_3$Ga$_{0.5}$In$_{0.5}$C

it was found that the actual compound formed is Mn$_3$Ga$_{0.53}$In$_{0.47}$C also, C and In peak is found in the plots. It can be said that Indium atoms replace the Ga atoms at the A-site. The lattice parameter of the sample is close to the average of the lattice parameters of the parent compound.
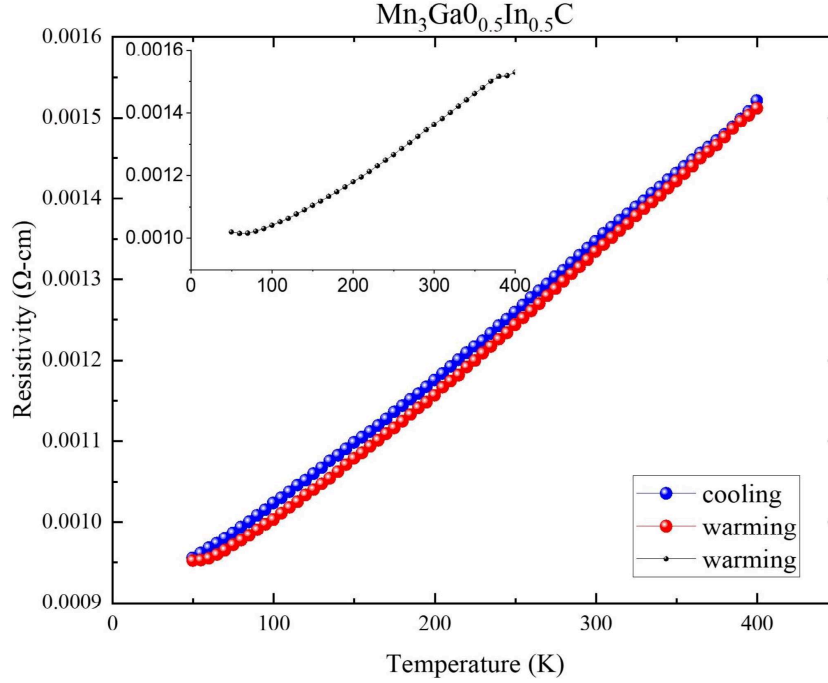
3.3.2   Resistivity

Figure 3.9: Resistivity vs Temperature plot for Mn$_3$Ga$_{0.5}$In$_{0.5}$C

The temperature dependent resistivity measurements carried out to understand the transport behaviour 3.9, showed overall a metallic behaviour and some transition can be seen in the first warming cycle. The data was recorded between the temperature range 50K to 400K.

3.4   Mn$_3$GaC Single crystal

3.4.1   SEM

Formation of Mn$_3$GaC single crystals is confirmed from the SEM measurements 3.10 and it is also confirmed from the single crystal XRD measurements. Single crystal XRD measurements were carried out on Bruker Smart Apex CCD diffractometer with graphite monochromated Mo K$_\alpha$ radiation (λ =0.71073 Å). The image taken using the video camera 3.11 shows the selected single crystal for the measurements. The size of the selected single crystal is about

50 microns. Figure 3.11 shows the hkl reflections observed after mounting the sample in the single crystal XRD diffractometer.
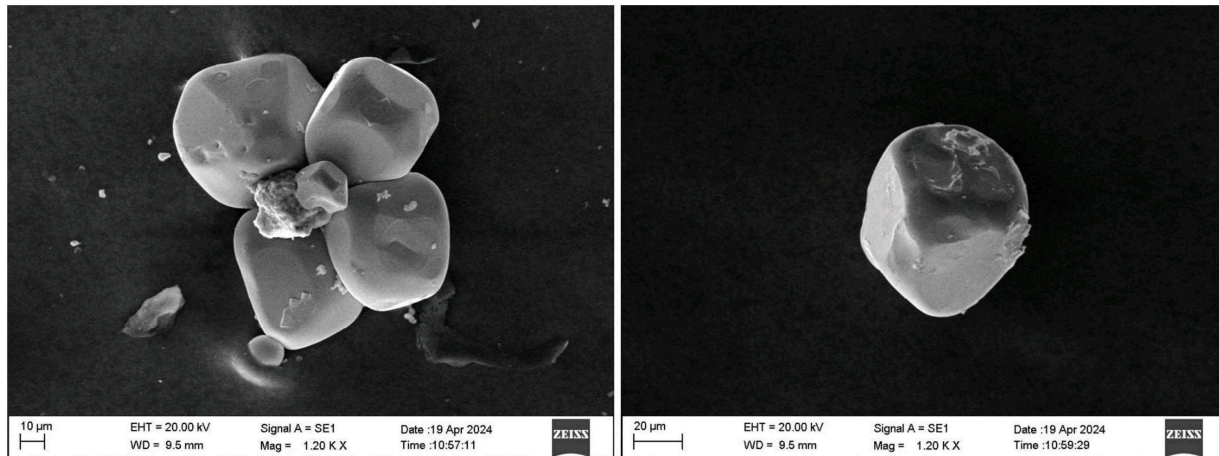

Figure 3.10: SEM image of Mn_3GnC single crystal

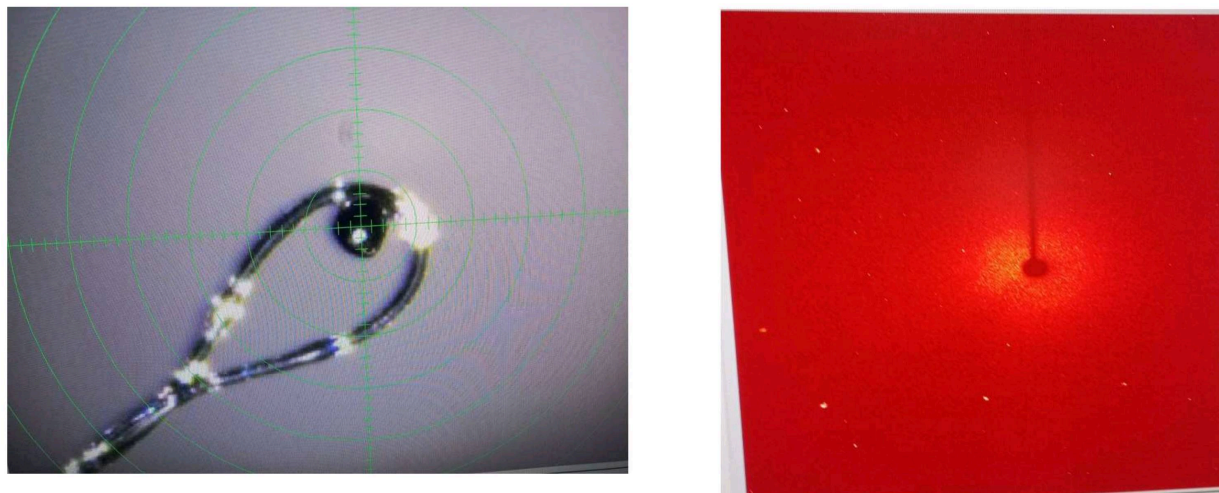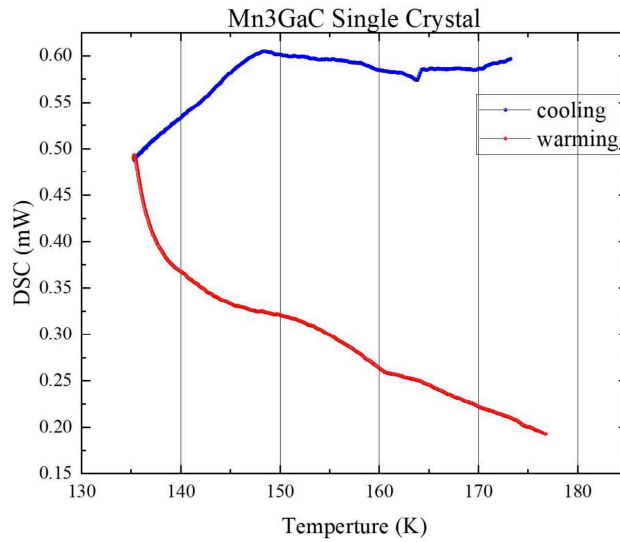## 3.4.2   Single crystal XRD measurement

Figure 3.11: Single crystal of Mn$_3$GaC anf hkl reflections observed

Single crystal XRD of Mn$_3$GaC was done at room temperature after refining the structure using Olex2.0 and using mercury software the lattice parameter is a = 3.8964(5)Å, it crystallises in cubic structure with space group Pm$\bar{3}$m. The lattice parameter is close to that reported for carbon-deficient compound reported in the literature[3].
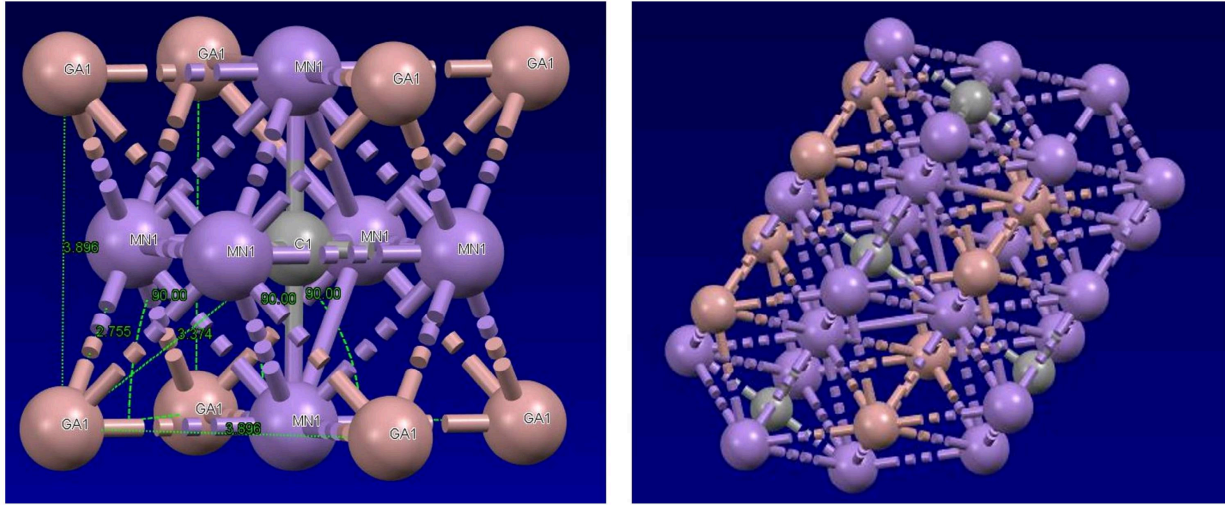
Figure 3.12: Single crystal structure of Mn₃GaC

Using the Mercury software the bond angles and bond lengths are measured as follows shown in the figures 3.14: Bond angle: Ga-Ga-Ga: 90°, Bond lengths: Ga-Ga = 3.896Å= lattice parameter, Ga-Mn = 2.755 ÅGa-C = 3.374 Å

3.4.3 DSC measurement

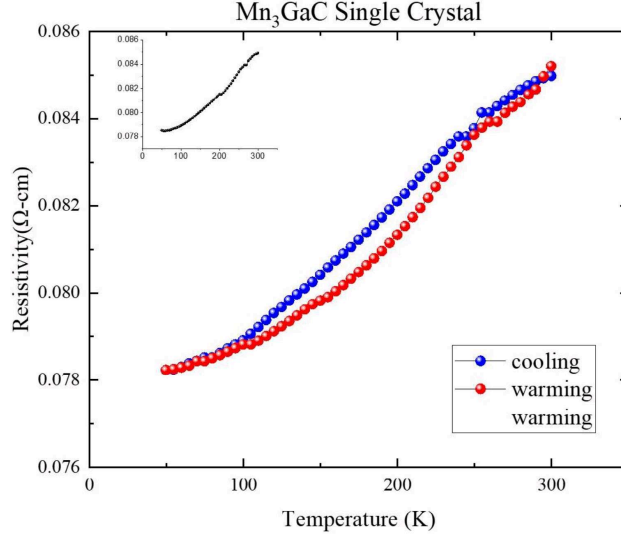Figure 3.13: DSC vs Temperature plot for single crystal Mn₃GaC

Figure 3.14: Resistivity vs Temperature plot for Mn$_3$GaC single crystal

Figure 3.13 shows DSC measurements were done on the sample no characteristic of first-order transition could be seen. As reported in the literature, the carbon-deficient compound does not exhibit first-order transition so, no peaks are observed in the DSC measurements. [4]

3.4.4   Resistivity

The resistivity vs temperature plot shows overall a metallic behaviour. The resistivity data was recorded in the temperature range of 50K to 300K. This sample is prepared by the slow cooling method does not show any discontinuity with temperature. This behaviour of resistivity is exactly similar to that reported earlier for Mn$_3$GaC$_{0.8}$ polycrystalline sample[4].
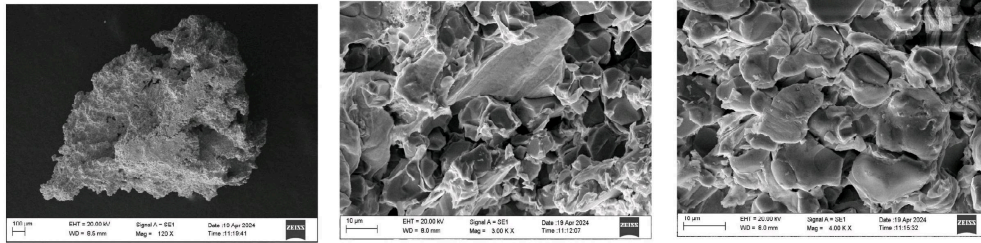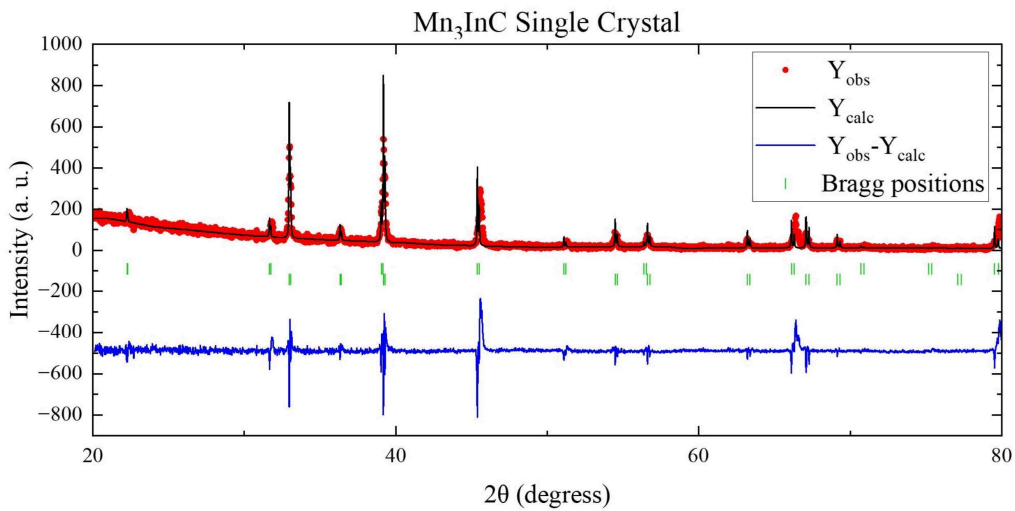
Figure 3.15: SEM images of Mn₃InC single crystal

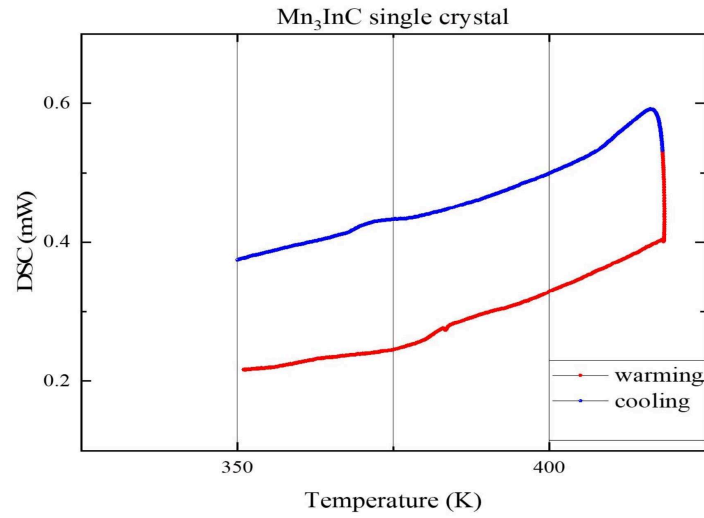## 3.5 Mn₃InC Single crystal

3.5.1 SEM

The SEM images 3.15 do not show the formation of any face of the crystal, this suggests the compound formed must be a polycrystalline sample. The reason it did not form single crystals might be because it was pressed into a pellet before sintering.

3.5.2 Le Bail Refinement

Figure 3.16: Le Bail refinement for Mn₃InC Single crystal

XRD data was recorded at room temperature from 2θ =20°to 80°in steps of 0.02°using Cu K_α radiation, wavelength $\lambda = 1.540560$Å. Mn₃InC crystallises in cubic phase with space

Figure 3.17: DSC vs temperature plot for Mn$_3$InC single crystal

group Pm$\bar{3}$m as reported in the literature with lattice parameter a = 3.99398(3)Å3.16. In this plot, no graphite peak was identified, and the impurity phases observed are of Indium only.

3.5.3 DSC measurement

The DSC plot 3.17 shows a broad transition as reported in the literature near the transition temperature in the literature[4].
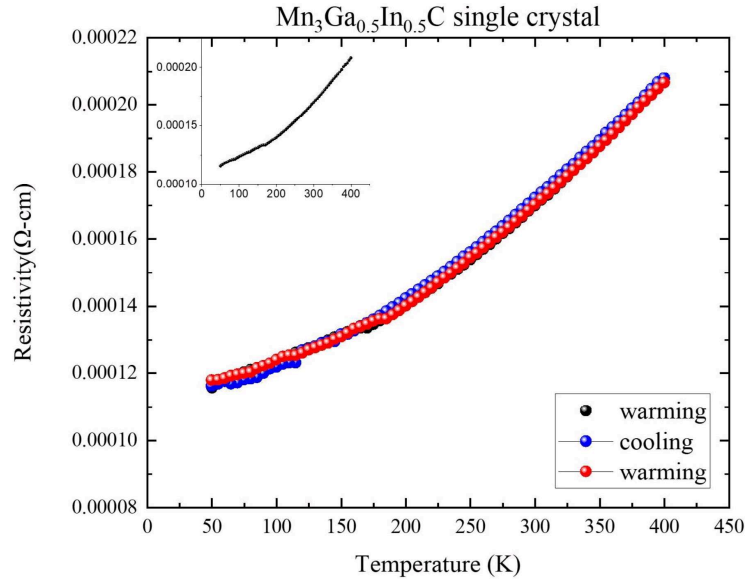
3.6 Mn$_3$Ga$_{0.5}$In$_{0.5}$C Single crystal

Le Bail refinement

The XRD measurements were done at room temperature in the range 2θ from 20°to 80°in the steps of 0.02 °using CuK$_\alpha$ radiation, wavelength λ = 1.540560Å. Le Bail refinement 3.18 of the sample was done, the compound crystallises in cubic structure with space group Pm$\bar{3}$m, lattice parameter a = 3.94648(3)Åwhich agrees with the polycrystalline sample. Along with Mn$_3$Ga$_{0.5}$In$_{0.5}$C phase Mn$_3$GaC, In and MnO impurities were present in the sample.
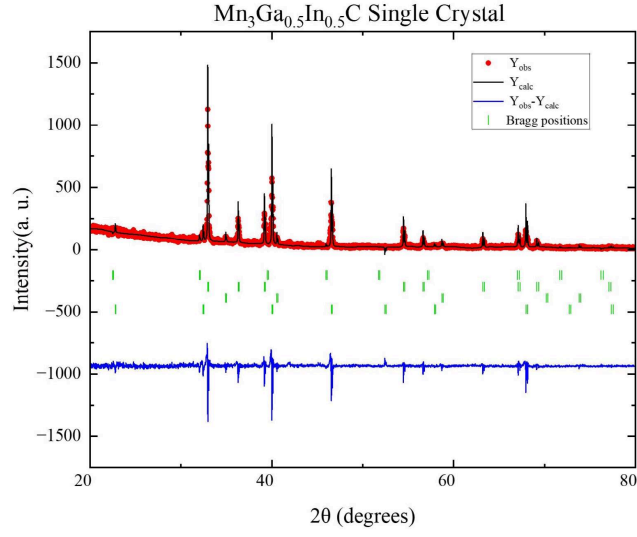
Figure 3.18: Le Bail refinement for Mn$_3$Ga$_{0.5}$In$_{0.5}$C

3.6.1   Resistivity

Figure 3.19: Resistivity vs Temperature plot for Mn$_3$Ga$_{0.5}$In$_{0.5}$C single crystal

To study the transport properties, temperature dependent resistivity was The resistivity vs temperature plot 3.19 shows overall a metallic behaviour, the behaviour is similar as that

observed on the polycrystalline sample. Also, the data was recorded in the temperature range of 50K to 400 K.

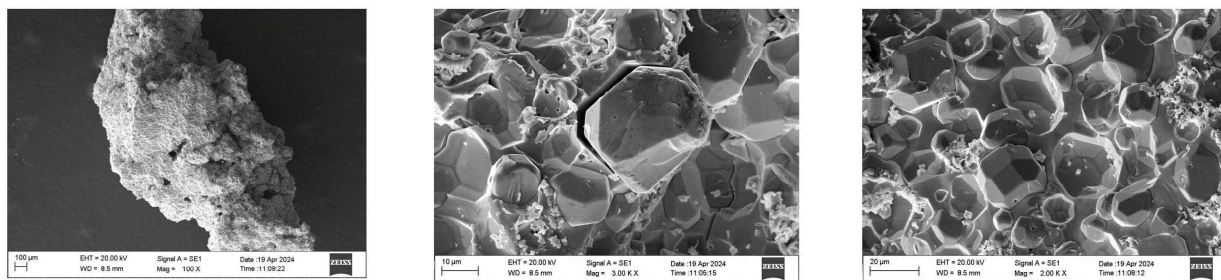## 3.7 Mn$_3$SnC Single crystal

3.7.1 SEM

Figure 3.20: SEM images of Mn$_3$SnC single crystal

The next compound studied is Mn$_3$SnC Single crystal. The formation of single crystals can be seen from the SEM images 3.20. However the size of the crystals formed is very small.

3.7.2 Le Bail Refinement

The XRD patterns were recorded at room temperature from $2\theta = 20°$ to $90°$ in steps of $0.02°$ using CuK$_\alpha$ radiation, wavelength $\lambda = 1.540560$Å. From Le Bail refinement 3.21 it can be seen that the compound crystallises in cubic structure as reported in the literature with space group Pm$\bar{3}$m along with impurity phases for Sn, SnO. The lattice constant is a=3.99652(4)Å[2].

3.7.3 DSC measurement

The DSC plots show dip and peak near the transition temperature as reported in the literature[4]. The hysteresis between the peaks suggests that the transition is of the first
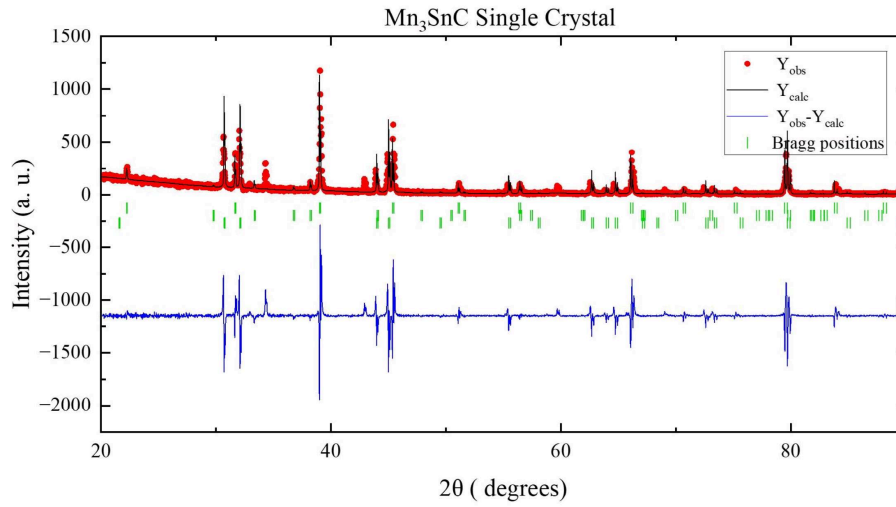
Figure 3.21: Le Bail refinement for Mn$_3$SnC Single crystal
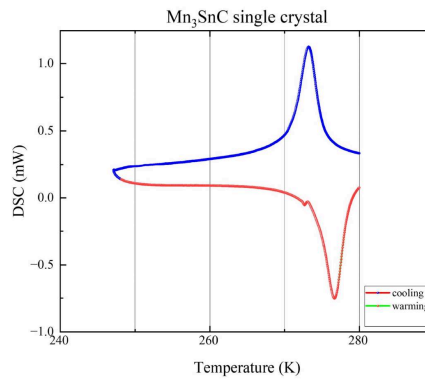
Figure 3.22: DSC vs Temperature plot for Mn$_3$SnC

order. The crystals would have grown bigger in size if the compound would have not been pressed into a pellet before the heat treatment.

Chapter 4

Conclusion

In this project, we tried to synthesise and characterise polycrystalline and single crystals of Mn_3GaC, Mn_3InC and $Mn_3Ga_{0.5}In_{0.5}C$ and single crystals of Mn_3SnC. All the compounds were prepared using the solid-state reaction method. The polycrystalline compounds were furnace-cooled and self-flux and slow-cooling methods were used for the synthesis of single crystals. XRD measurements were done on the samples to check the purity, the expected outcome was that the compounds would form a single phase but impurity phases were present. To check the formation of single crystals, SEM measurements were done on the compounds. It turned out that single crystals of only Mn_3GaC, Mn_3SnC were formed. The size of Mn_3GaC single crystal was about 50 microns single crystal XRD measurements were done on this sample, while the size of Mn_3SnC single crystals was very small to carry out single crystal XRD measurements. To study the transport properties, temperature-dependent resistivity measurements were done, and all the compounds overall showed metallic behaviour. Also, DSC measurements were done on the single crystals to check the presence of first-order transition in the sample formed. The self-flux and slow cooling methods can be used to grow single crystals of these compounds.

Bibliography

[1] Fabian Burkhardt. *The Crystal Structure of the New Ternary Al8Cr4Sc Phase in the Al-Cr-Sc Push-Pull Alloy.* PhD thesis, 04 2018.

[2] Elaine T Dias. *Study of Magnetoelastic Coupling in Antiperovskite Materials.* PhD thesis, Goa University, 2017.

[3] ET Dias, KR Priolkar, and AK Nigam. Effect of carbon content on magnetostructural properties of mn3gac. *Journal of magnetism and magnetic materials*, 363:140–144, 2014.

[4] ET Dias, KR Priolkar, Rajeev Ranjan, AK Nigam, and S Emura. Mechanism of magnetostructural transformation in multifunctional mn3gac. *Journal of Applied Physics*, 122(10), 2017.

[5] ET Dias, A Das, A Hoser, S Emura, AK Nigam, and KR Priolkar. Absence of first order magnetic transition, a curious case of mn3inc. *Journal of Applied Physics*, 125(6), 2019.

[6] ET Dias, KR Priolkar, A Das, G Aquilanti, Öznur Çakir, M Acet, and AK Nigam. Effect of local structural distortions on magnetostructural transformation in mn3snc. *Journal of Physics D: Applied Physics*, 48(29):295001, 2015.

[7] VN Gaonkar, ET Dias, Arka Bikash Dey, Rajendra Prasad Giri, AK Nigam, and KR Priolkar. Role of tin and carbon in the magnetic interactions in mn3snc. *Journal of Magnetism and Magnetic Materials*, 471:215–219, 2019.

34

[8] ET Dias, KR Priolkar, Ö Çakir, M Acet, and AK Nigam. Effect of composition on magnetocaloric properties of mn3ga (1- x) snxc. *Journal of Applied Physics*, 117(12), 2015.

[9] ET Dias, KR Priolkar, AK Nigam, R Singh, A Das, and G Aquilanti. Phase-separated magnetic ground state in mn 3 ga 0.45 sn 0.55 c. *Physical Review B*, 95(14):144418, 2017.

[10] ET Dias, A Das, A Hoser, S Emura, AK Nigam, and KR Priolkar. Phase separation and effect of strain on magnetic properties of mn sub (3) ga sub (1-x) sn sub (x) c. 2018.

[11] F Scheibel, B Zingsem, T Feggeler, R Meckenstock, D Spoddig, M Farle, and M Acet. Magnetic anisotropy of single-crystal antiperovskite mn 3 gac studied by ferromagnetic resonance and dynamic magnetic-response simulations. *Physical Review Materials*, 3(5):054403, 2019.

[12]

[13] X-Ray diffractometer and its various component parts for X-Ray studies — xrd.co. `https://xrd.co/component-parts-x-ray-diffractometer/`.

[14] Homepage of Pranab Das — pranabdas.github.io. `https://pranabdas.github.io/research/fullprof/`.

[15] Bernard Dennis Cullity. *Elements of X-ray Diffraction*. Addison-Wesley Publishing, 1956.

[16] Anwar Ul-Hamid. *A beginners' guide to scanning electron microscopy*, volume 1. Springer, 2018.

[17] Weilie Zhou, Robert Apkarian, Zhong Lin Wang, and David Joy. Fundamentals of scanning electron microscopy (sem). *Scanning microscopy for nanotechnology: techniques and applications*, pages 1–40, 2007.

[18] Differential Scanning Calorimeters (DSC) — ssi.shimadzu.com. `https://www.ssi.shimadzu.com/products/thermal-analysis/` `differential-scanning-calorimeters/index.html`.